

Characterizing width uniformity by wave propagation

Luciano da F. Costa* and Giancarlo Mutinari

Cybernetic Vision Research Group, IFSC—University of Sao Paulo, Caixa Postal 369, Sao Carlos, SP 13560-970, Brazil

David Schubert†

Salk Institute, 10010N Torrey Pines Road, La Jolla, California 92037, USA

(Received 11 April 2003; published 13 November 2003)

This work describes a different image analysis approach to characterize the uniformity of objects in agglomerates by using the propagation of normal wave fronts. The problem of width uniformity is discussed and its importance for the characterization of composite structures normally found in physics and biology highlighted. The methodology involves identifying each cluster (i.e., connected component) of interest, which can correspond to objects or voids, and estimating the respective medial axes by using a recently proposed wave front propagation approach, which is briefly reviewed. The distance values along such axes are identified and their mean and standard deviation values obtained. As illustrated with respect to synthetic and real objects (*in vitro* cultures of neuronal cells), the combined use of these two features provides a powerful description of the uniformity of the separation between the objects, presenting potential for several applications in material sciences and biology.

DOI: 10.1103/PhysRevE.68.056704

PACS number(s): 07.05.Pj

I. INTRODUCTION

Structures defined by the agglomeration of basic elements are often characterized by the presence of objects and voids defined between the former. Figure 1 illustrates such a situation with respect to neuronal cells grown *in vitro* on different substrata, namely, fibronectin (a) and tissue culture plastic (b). Several important properties of such structures can be inferred from the geometry of the objects and voids present in such images, which has motivated the growing use of imaging methods in physics and in biology (e.g., Refs. [1–4]). For example, the migration of nerve and glial cells and axon elongation in the developing nervous system lead to different patterns of cell agglomeration and separation [5]. In material sciences, the geometrical properties of the voids have strong influence over the respective mechanical and electrical properties of the composite and can tell much about the composite formation process. The present work describes a different concept and methodology for characterizing the width uniformity of the objects or voids in such agglomerates.

The first important point is to properly and accurately characterize what is meant by uniformity of objects or voids. A possible interpretation would regard how these elements distribute themselves along the composite space. We could be interested, for example, in quantifying their translational invariance, a problem that could be suitably tackled by using the lacunarity measure described in Refs. [1–3]. The alternative problem considered in the present work is to quantify the uniformity of the width of objects or voids. Figure 2 illustrates such a situation with respect to two hypothetical structures chosen for didactical purposes. The agglomerate in (a) presents a single void (the black connected region) and

objects (in white) that have similar widths, while the case in (b) provides a nonuniform collection of objects. The importance of quantifying the kind of width uniformity seen in (a) is particularly relevant because it may provide valuable information about the processes intrinsically related to the composite formation as well as about the interactions between the basic elements of the composite. Ideally, it would be interesting to have a single uniformity index that could be assigned to each agglomerate image. The current work proposes an effective solution to such a problem that can be extended also for analysis of connected components (i.e., objects or voids) involving connected holes such as the voids in the two situations in Fig. 2.

Firmly based on concepts from mathematics and physics, wave front propagation approaches have been extensively used for several purposes in image analysis and applications (e.g., Refs. [6,7]). Typically, such methods involve the propagation, along the object contour normal of a wave front, starting from the object of interest, in such a way that shocks between portions or individual fronts are obtained. A shock is henceforth understood as the collision between two different points along the propagating wave front(s). Medial axes are often defined as the set of points corresponding to the centers of bitangent circles maximally inscribed into the object of interest, which therefore coincide with the shock points. Also known as skeletons, such axes can be informally said to correspond to the “middle” part of the objects (see Fig. 6). Although alternative approaches to medial axes estimation (e.g., Ref. [8]) can be used, the current work considers the numeric approach developed in Refs. [9–11], which also allows a spatial scale parameter controlling the degree of detail of the obtained axes. While simpler skeletonization algorithms have been reported in the literature, such algorithms do not guarantee unit width or full connectivity. For instance, skeletons produced by distance-based schemes such as that reported in Ref. [12] can result disconnected, as is the case for dumbbell-like shapes.

*Email address: luciano@ifsc.usp.br

†Email address: schubert@salk.edu

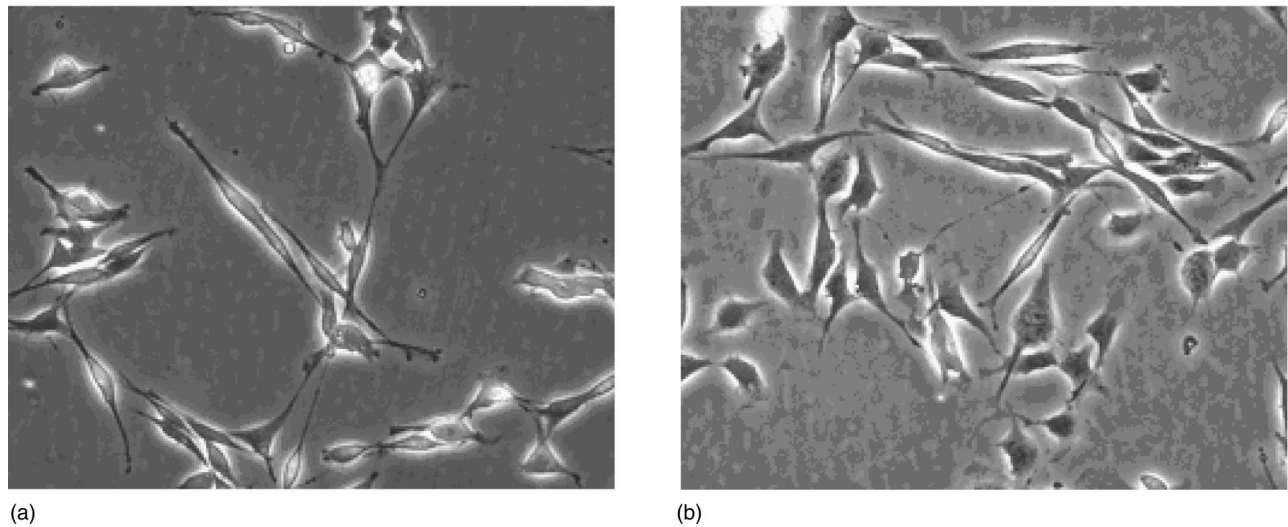


FIG. 1. Neuronal cells grown on different substrata, namely, fibronectin (a) and tissue culture plastic (b).

The basic principle underlying the method for quantifying width uniformity described in the current paper is the fact that the distance values along the medial axes provide a natural characterization of the width distribution of objects even when they are not straight or present ramifications and holes. The potential of the use of the distances along the medial axes is illustrated in Fig. 3. Any object in this figure is characterized by the peculiar situation that the same distance value is found along the respective medial axes. The concept of width can therefore be extended from straight objects to a more general set of shapes, including those that are curved or present branches. In brief, all shapes in Fig. 3(a) can be said to have the same width. This class of objects has been studied in Ref. [13] under the name of polyballs. While such objects with constant width represent a somewhat limited class of possible objects, the concept of width can be immediately extended to more general shapes by considering the distance value along the object medial axes. Figure 3(b) illustrates such an approach with respect to a more generic object. The distances d along the respective medial axis represented by the dashed line provide a natural means to characterize the widths of distribution of the object.

Such distributions of distances along the medial axes are henceforth taken as an accurate indication about the object

width. While the histogram of the distances along the medial axes of all objects (or voids) in the agglomerate could be taken as a more comprehensive statistical model for characterizing the object width, we restrict our attention to its mean and standard deviation, represented henceforth as \bar{w} and σ_w , as well as the correlation coefficient v between these two measurements. Given its adimensional nature, the latter provides a particularly interesting candidate for quantification of the uniformity of the object's width. As will be illustrated in this paper, these three measures provide meaningful and comprehensive geometrical characterization of the objects or voids in agglomerates not only in terms of width uniformity, but also as far as the size of those objects is concerned. This

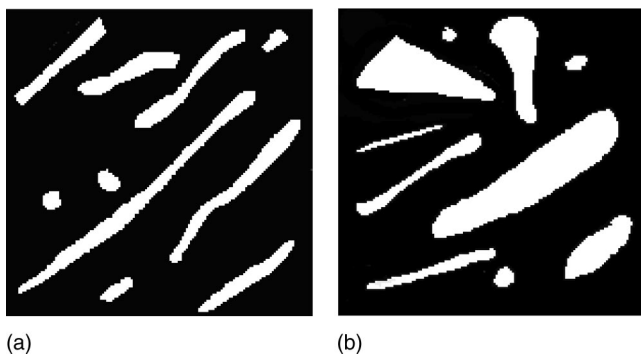


FIG. 2. Two types of agglomerates exhibiting different width uniformity of objects (represented in white).

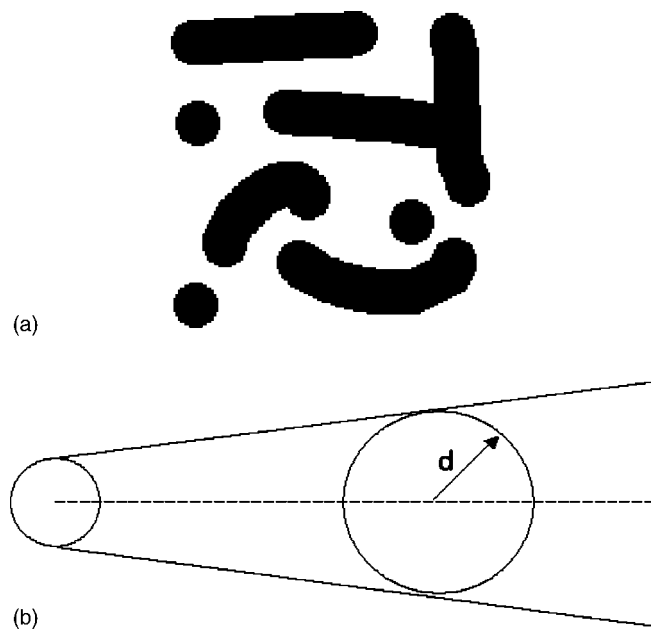


FIG. 3. Several objects characterized by the same distances along their respective medial axes (a). The generalization of the width of a generic object in terms of the distances along medial axes (b).

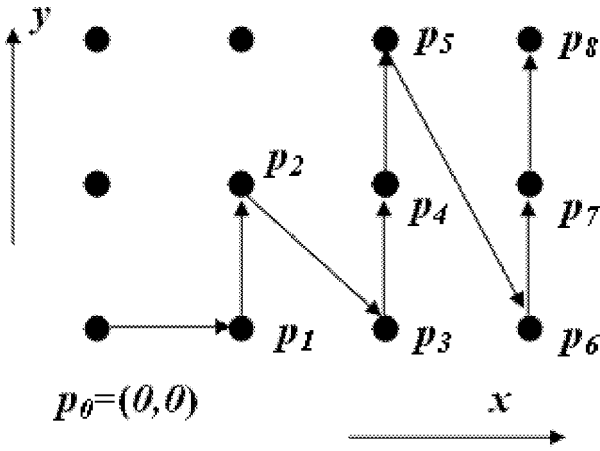


FIG. 4. The sequence of lattice points $p_i=(x,y)$ defining the first nine exact distances $d_i=\sqrt{x^2+y^2}$.

paper starts by presenting the methodology suggested to estimate the medial axes and distances, leading to the three width features \bar{w} , σ_w , and v . Next, the potential of these measures to quantify width uniformity is illustrated with respect to synthetic and real data corresponding to agglomerates of neuronal cells grown over four different types of substrata.

II. METHODOLOGY

Given an image of an agglomerate characterized by objects over a background (or any two distinct phases) like that in Fig. 2(b), the first step of the proposed methodology involves identifying all connected components for the object or voids. A connected component is understood as the set of all pixels that are connected to its four or eight neighbors [11]. This work adopts four-neighborhood. In case we are analyzing voids, a single connected component is obtained for the agglomerates in Fig. 2. At the same time, a total of ten connected components are obtained in case we are interested in the objects. The extraction of the connected components can be done by using standard region growing or inundation algorithms (e.g., Ref. [11]). Let P be any of the points of the component to be extracted. Such methods search for the neighbors N of P that have the same pixel value as P . The procedure is repeated for the neighbors N until no more neighbors with the same pixel value are found. Once the connected components have been obtained, we need to estimate the multiscale medial axes of each of them. This procedure is illustrated with respect to one of the void connected components from the agglomerate in Fig. 2(b), shown in Fig. 5(a). First, the border of the connected component is extracted in a clockwise or counterclockwise fashion. Traditional algorithms for border extraction (e.g., Ref. [11]) are used in the present work. The output of such algorithms is a spatially quantified parametric curve defined by the list of ordered coordinates $x(i), y(i)$, where $i=1, 2, \dots, N$ is the curve parameter corresponding to the order the border elements are visited by the border extraction procedure. Figure 5(c) illustrates a portion of the extracted border of the connected component in (a), parametrized by integer values cor-

responding to the sequence in which the border was followed. The arc length $s(i)$ along such a curve is then accurately estimated by using the spectral method described in Ref. [11]. This method involves obtaining the Fourier series for the parametric curve defined by the extracted border and calculating the derivatives by using the property $\dot{x} \leftrightarrow \mathcal{J}^{-1}\{(2\pi if)\mathcal{J}(s)G_\sigma\}$, where \mathcal{J} is the Fourier transform and G_σ is the Fourier transform of the unit area Gaussian smoothing function $G_\sigma=1/(\sigma\sqrt{2\pi})\exp\{-0.5(x/\sigma)^2\}$ with standard deviation σ . The arc length can be immediately obtained from the calculated derivatives as $s(i)=\sum_{k=1}^i\sqrt{\dot{x}^2(i)+\dot{y}^2(i)}$. Additional information about derivative estimation through spectral methods can be found in Ref. [11]. The value of σ is henceforth fixed at seven pixels, which minimizes the effect of the spatially quantized nature of the curve—recall that in digital images such curves are represented over the orthogonal lattice—without excessively affecting (smoothing) the curve. The estimated arc length for the object in Fig. 5(a) is given in panel (d). Having obtained the border of the connected component reparametrized in terms of its arc length, a wave front is propagated from the border, unfolding with constant speed and normal orientation. The shocks implied by such a traveling wave front as a consequence of curvature variations along the object geometry define the medial axis of the connected component under analysis. The methodology proposed in Refs. [9–11], and reviewed below, is used in this work for such a purpose. The basic idea of this method is to propagate circular waves centered at each of the contour elements, according to the Huyghens principle of wave propagation. Constant radial speed is assumed. Given that the objects in digital images are represented over the orthogonal lattice, which implies specific anisotropies, it is necessary to consider only those distances that are representable in such spaces, which are called *exact distances*. Figure 4 illustrates the sequence of lattice points $p_i(x,y)$, $i=0, 1, \dots, 8$, corresponding to the nine initial exact distances $d_i=\sqrt{x^2+y^2}$. Once such distances have been precalculated (see Ref. [11]) and stored jointly with the respective relative position vectors with respect to the origin, the algorithm consists in visiting each of the border elements for each subsequent exact distance, and updating the empty cells indexed by the respective relative positions with the current distance value or the respectively associated arc length. In the former case, the resulting image corresponds to the distance transform of the object, which associates to each surrounding pixel the smallest Euclidean distance to the object. In case the arc length is updated, we get a labeled image that can be further processed in order to obtain label differences (see Refs. [10,11]) corresponding to the intensity of the shocks between different portions of the traveling wave front. Figures 5(e) and 5(f) illustrate the distance transform and propagated labels obtained for the object in panel (a).

By thresholding the difference image with different values T , it is possible to obtain a family of medial axes with varying degrees of detail. The higher the value of T , the more the details are filtered out. The application of the above methodology for medial axes estimation to the problem of width

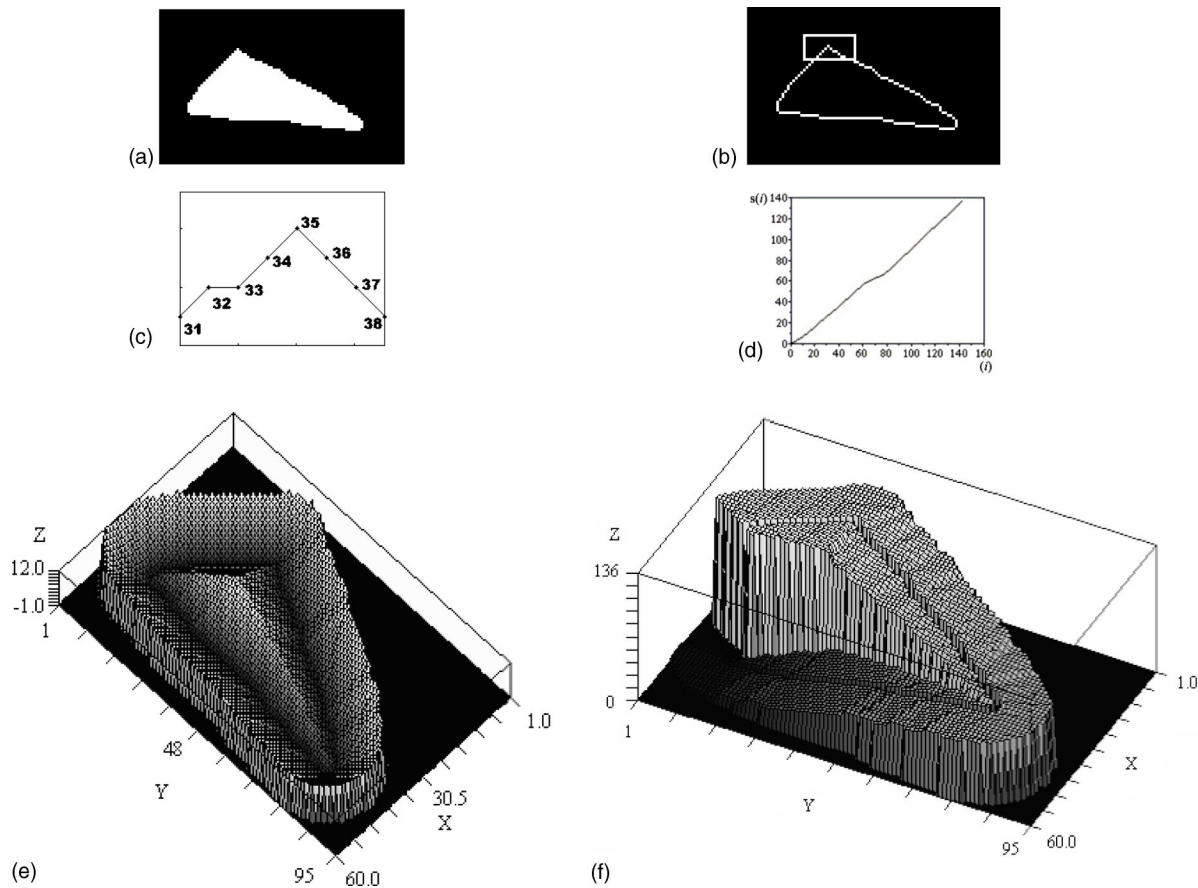


FIG. 5. Illustration of the multiscale medial axes estimation by using level sets. The original connected component (a), its extracted border (b), parameter values along a piece of such a border (c), arc length along the parametrized contour (d), distance transform (e), and propagated labels (f).

uniformity involves selecting a suitable value of T so as to remove unimportant small scale detail such as vertices along the object. Figure 6 illustrates several medial axes obtained for varying values of T . The specific choice of the threshold value should take into account the resolution and specific demands imposed by each application.

If connected component presents holes, as is the case with the composites in Fig. 1, each hole has to be identified by using border extraction algorithms and labeled individually with specific labels (i.e., a single distinct label is assigned to each border). By applying the wave propagation method to such borders, the generalized Voronoi diagram of the borders is obtained, and the multiscale medial axes are then calculated inside each of the Voronoi cells by using the same method described above [14]. The generalized Voronoi diagram corresponds to a partition of the image space in such a way that all points in each region are closest to the respective object (one of the image connected component) than to any other object. Recall that the distance between a point and an object is defined as the smallest distance between the point and any of the points composing the object. Figure 7 illustrates the generalized Voronoi diagram and the distance values along the borders (fixed-scale medial axes) determined by the Voronoi cells.

At this point, it is possible to derive a distance weighted medial axis by assigning to each point of the selected medial

axes the respective distance transform values. The set of distance values found along the medial axis are henceforth called *medial axis distances* or *skeleton distances*. The methodology for width uniformity characterization involves the consideration of the distance values along all the medial axes in the agglomerate. The mean and standard deviation of the distances over every medial axis point of the object are then estimated. Table I gives these values, as well as the correla-

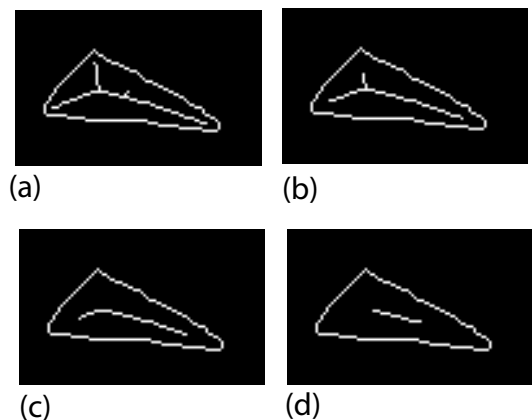


FIG. 6. Medial axes obtained for $T=5$ (a), 10 (b), 20 (c), and 50 (d).

TABLE I. The mean, standard deviation, and correlation coefficient obtained for the voids and objects with respect to the two composites in Fig. 1.

	\bar{w}	σ_w	v
Figure 1(a), Objects	2.06	0.62	0.30
Figure 1(a), Voids	6.57	3.71	0.57
Figure 1(b), Objects	4.37	2.29	0.52
Figure 1(b), Voids	6.09	3.25	0.54

tion coefficient, for the two images in Fig. 2 considering objects and voids.

Several interesting facts result, or can be inferred from such measures. To start with, the mean width \bar{w} obtained for the objects (cells) in Fig. 2(a) is less than half of the value obtained for the objects in Fig. 2(b), which is in full agreement with the visual interpretation of those images. At the same time, the mean widths obtained for the voids are similar in both images. The standard deviations obtained for the objects in those images are also in full agreement with the fact that the width dispersion of the objects in (a) is much smaller than that characterizing (b). Similar values are obtained for the voids. The coefficient of variation (v) provides an adimensional characterization of the observed width dispersion differences for the composites in Fig. 2.

III. APPLICATION TO NEURONAL AGGLOMERATES

During the development of the nervous system the distribution and connections of cells is determined by a variety of factors, including the adhesion of cells and axons to extracellular matrix material such as laminin and fibronectin [5]; little is known, however, about the determinants of cell shape. Some aspects of cell-matrix adhesions and their relationship to cell shape can be studied *in vitro* by plating nerve cells derived from a single common precursor cell (clonal cells) on different surfaces and asking how the different surfaces regulate the morphology of the cell. Figure 8 shows that there are great differences in the shape of a clonal nerve cell line called B103 grown on polylysine, laminin, fibronectin, and tissue culture plastic. 400×319 pixel images of the

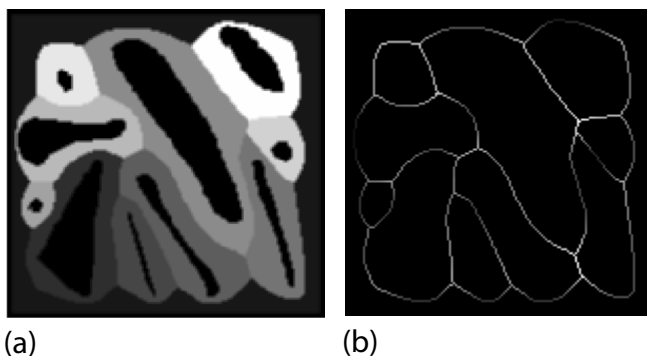


FIG. 7. The generalized Voronoi diagram (b) for the composite in Fig. 1(b) and the respective distance transform values (a) obtained along the Voronoi borders.

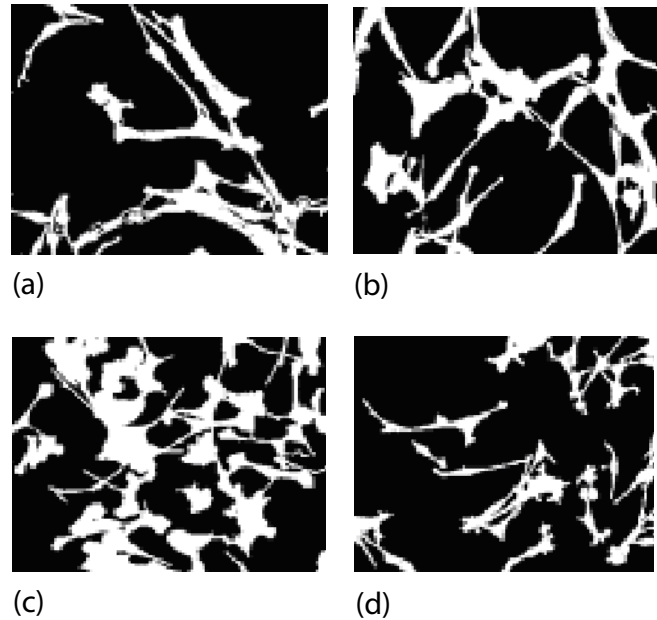


FIG. 8. Binary images (after segmentation of the neuronal cells, shown in white, consequently, the voids are black) showing examples of neuronal agglomerates grown on different substrata and respective values of \bar{w} and σ_w . (a) Fibronectin, (b) laminin, (c) tissue culture plastic, and (d) polylysine.

cultured cells were obtained by using a Leitz DMIRB inverted microscope and an Openlab (Leica) image acquisition system connected to a personal computer. Cell shape can be assigned a numerical value and questions can be asked about how the shape of cells grown on the different substrata differ from each other. The original gray-level images, such as those illustrated in Fig. 1, were segmented [11] in order to separate the cells from the substrate, yielding binary images where the voids are marked as “0” and the cells (or objects) as “1.” Attention is concentrated on the analysis of void uniformity. The segmentation was performed by automated segmentation (thresholding) followed by manual editing of the obtained structures in order to remove artifacts such as the presence of spurious particles and shadows. Figure 8 presents examples of binary images obtained by the segmentation methodology described above. Each of the connected voids were isolated by using a standard region growing approach [11], and the multiscale medial axes were obtained by using the level set-based approach as described in Sec. II. Specific medial axes were obtained by selecting the spatial scale to 10.

Figure 9 shows the phase space (or scatter plot) obtained by considering the mean and standard deviation of the void medial axes distances. The first important feature in this plot is the relatively strong overall correlation coefficient (namely, 0.86) between the two considered measures. While an almost linear separation was obtained between classes 3 (laminin, triangles) and 4 (polylysine, circles), the other two classes led to more dispersed, overlapped clusters. Regarding the mean values of \bar{w} calculated for each class, we find (mean of \bar{w}_3) < (mean of \bar{w}_2) < (mean of \bar{w}_1), indicating that the cells grown over these types of substrates tend to be

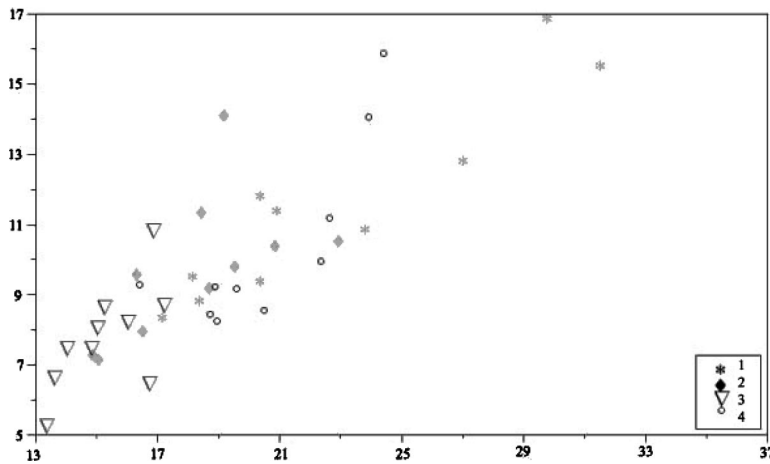


FIG. 9. Scatter plot showing the distribution of the neuronal agglomerates. The clusters obtained for classes 3 and 4 are clearly linearly separable, while the other clusters are characterized by substantial overlap.

progressively less packed. This is probably a reflection of a competition between cell-cell and cell-substratum adhesion on each surface. Cells that adhere better to themselves than to the surface on which they are grown tend to aggregate or, in the case of neurons, form fascicles [15]. Therefore, cells grown on more adhesive surfaces such as tissue culture plastic would tend to be spread out on the surface, while those on less adhesive substrate would form clumps as observed in Fig. 8. The correlation coefficient obtained for each of the four clusters are, respectively, 0.91, 0.73, 0.84, and 0.87, indicating substantially distinct uniformities characterizing each substrate. Whereas the voids in class 1 are characterized by the highest width uniformity, those in class 2 exhibit the most heterogeneous widths (Fig. 9).

IV. CONCLUDING REMARKS

This paper has reported a different and comprehensive approach to characterizing width uniformity in objects and voids typically found in images of agglomerates. The methodology is based on the objective characterization of “object width” in terms of the distances found along its medial axes, which are obtained by using a wave front propagation scheme. In this way, it becomes possible to speak objectively about the width of a wide class of shapes, including those that are curved or present branches. Such an approach to width characterization is further enhanced by the fact that most objects can be approximated or decomposed into varying radii polyballs. An accurate numerical approach has been adopted for the estimation of the medial axis distances,

which involves object isolation, border extraction, arc length reparametrization through a spectral approach, and the calculation of multiscale medial axes by using wave front propagation. Several of these methods were only recently described in the literature and are applied in combined fashion for width estimation in the present work. The potential of the proposed framework was illustrated and corroborated with respect to synthetic agglomerate images and real data concerning neuronal cells grown on different substrata. By examining a clonal nerve cell line grown on different protein substrata it was possible, using this methodology, to quantify the morphological differences caused by the different substrata. It is shown that when nerve cells are grown on different surfaces, there is a dramatic correlation between the shape of the obtained voids and the tendency of the cells to associate between themselves. The use of the above methodology combined with complementary agglomerate measures such as the fractal dimension and lacunarity provide the potential for a rich and comprehensive characterization of the geometry of the shapes and agglomerates of both biological and physical objects. Finally, it is interesting to note that the above proposed methodology for characterizing the width of objects can be immediately extended to three-dimensional (3D) data, such as those obtained from magnetic resonance imaging. However, the extraction of 3D medial axes is substantially more demanding, and skeletonization schemes such as those reported in Ref. [16], which rely on graph geodesics, would be required in those cases in order to obtain suitable medial axes.

-
- [1] A.J. Einstein, H.S. Wu, and J. Gil, *Phys. Rev. Lett.* **80**, 397 (1998).
 - [2] J.P. Hovi, A. Aharony, D. Stauffer, and B.B. Mandelbrot, *Phys. Rev. Lett.* **77**, 877 (1996).
 - [3] B.B. Mandelbrot, *The Fractal Geometry of Nature* (Freeman, New York, 1983).
 - [4] R.E. Plotnick, R.H. Gardner, W.W. Hargrove, K. Prestegard, and M. Perlmutter, *Phys. Rev. E* **53**, 5461 (1996).
 - [5] B.J. Dickson, *Science* **298**, 1959 (2002).
 - [6] S. Osher and J.A. Sethian, *J. Comput. Phys.* **79**, 12 (1988).
 - [7] J.A. Sethian, *Level Set Methods and Fast Marching Methods: Evolving Interfaces in Computational Geometry* (Cambridge University Press, Cambridge, 1999).
 - [8] R.L. Ogniewicz and O. Kubler, *Pattern Recogn.* **28**, 343 (1995).
 - [9] L.F. Costa, in *Proceedings of the International Workshop on Synthetic-Natural Hybrid Coding and Three Dimensional Imaging*, edited by M. G. Strintzis and F. Lavagetto (Aristotle University, Santorini, 1999), pp. 214–217.
 - [10] L.F. Costa and L.F. Estrozi, *Electron. Lett.* **35**, 1829 (1999).

- [11] L.F. Costa and R.M.C. Junior, *Shape Analysis and Classification, Theory and Practice* (CRC Press, Boca Raton, FL, 2001).
- [12] P.E. Danielsson, *Comput. Graph. Image Process.* **14**, 227 (1980).
- [13] P. Attali, D. Bertolino, and A. Montanvert, in *Proceedings of the International Conference on Pattern Recognition*, edited by L. Shapiro and S. Tanimoto (IEEE, Seattle, 1994), pp. 626–628.
- [14] A.X. Falcao, L.D. Costa, and B.S. Da Cunha, *Pattern Recogn.* **35**, 1571 (2002).
- [15] D. Schubert and F.G. Klier, *Fasciculation Brain* **549**, 305 (1991).
- [16] A. Verroust and F. Lazarus, *Visual Comput.* **16**, 15 (2000).